Supplemental Material to

Physical transport of magmatic sulfides promotes copper enrichment in hydrothermal ore fluids

Published in GEOLOGY (2022) by Christoph A. Heinrich and James A.D. Connolly

Stokes calculations

T-X dependent viscosities of silicate magmas were calculated with the excel calculator available at https://www.eoas.ubc.ca/~krussell/VISCOSITY/grdViscosity.html Giordano et al. (2008; with thanks to Daniele Giordano, pers. comm, 2021).
P-T-X dependent melt densities were calculated with the calculator supplement to Iacovino and Till (2018; Supplementary File 1 at https://www.jvolcanica.org/ojs/index.php/volcanica/article/view/12). A fixed sulfide density of 4600 kg m^{-3} was used, ignoring compositional variations, the small P-T dependence of sulfide density (Nishida et al., 2011) and the composition-dependent melting of the FeS-rich phase (e.g., Kress et al., 2008). As sulfides observed in lower-crustal cumulates are interpreted to have been mostly solid (Chen et al., 2020; Du and Audétat, 2020), we use the Stokes formula for solids; liquid droplets might sink up to 1.5 times faster (cf. De Bremond d'Ars et al., 2001; Yao et al., 2019), an effect that is insignificant in light of parameter uncertainties. For the silicate melt, three compositions were considered, with additional 3 or 10% H_2O, normalised to 100 wt%:

Table S1: Average continental arc basalt composition from Rezeau and Jagoutz (2020) (left, used for thermodynamic and Stokes calculations) and the reference diorite (dacite) reported by Cox et al. (2020) (for Stokes calculations). For the thermodynamic modeling shown in Figures 2 and 3, minor MnO and P_2O_5 was neglected, the H_2O content was varied between 3 and 6% and Fe^{III}/Fe^{tot} was varied between 0.18 and 0.48.

	Continental arc basalt	BH-1 diorite / dacite
SiO_2	50.43	62.9
TiO_2	0.99	0.35
Al_2O_3	15.64	12.99
FeO^{tot}	8.56	4.76
MnO	0.14	0.13
MgO	10.24	2.25
CaO	9.86	2.76
Na_2O	2.79	3.04
K_2O	1.04	0.68
P_2O_5	0.26	0.07
H_2O	10 / 3 or 6	10.00
Fe^{III}/Fe^{tot}	0.18 - 0.48	

Magma ascent rates vary over many orders of magnitude depending on data source (U-Th-series disequilibrium data or speedometers based on component diffusion profiles between phenocryst, glass matrix or inclusions) and geological process or tectonic setting – see reviews by Turner and Costa (2007) and Neave and Maclennan (2020; many estimates extend to even higher flow rates than shown in Figure 1, especially in the upper crust).

Thermodynamic modeling

The Perple_X free energy minimization package package (Connolly, 2005, v. 6.9.1 of July 2021, https://www.perplex.ethz.ch) was used to compute phase relations in multicomponent model systems of fixed bulk composition, representing hydrous arc basalt with excess FeS. Mark Caddick (Virginia Tech) is thanked for its compilation for MacOS.

For the silicate melt we chose the multicomponent model of Holland et al. (2018). This model does not include S dissolved in the silicate melt, which has been modelled in many detailed experimental (e.g., Mavrogenes and O'Neill, 1999; Liu et al., 2007; Jugo, 2009; Fortin et al., 2015; Matjuschkin et al., 2016) and computational studies (e.g., Rottier et al., 2019; Chen et al., 2020; Yao and Mungall, 2020). In reality, $CaSO_4$ dissolved in silicate melt will replace some of the predicted anhydrite field in oxidized magmas. The solubility of FeS is more limited and solid FeS is stabilised to higher T and fO_2 with increasing total pressure (Matjuschkin et al., 2016).

Our results focus on the competition among solid sulfide, sulfate, and S dissolved in a magmatic molecular H-O-S fluid. We avoid sequential computing of the thermodynamics of FeO as a major schematic component, e.g., from initial calculations using MELTS (Ghiorso and Sack, 1995) followed by computation of fluid species via fO_2 or fS_2 (Mungall et al., 2015; Yao and Mungall, 2020). Although thermodynamically equivalent, calculation of overall multicomponent equilibrium by Gibbs energy minimization has the advantage of yielding quantities and compositions of all mineral, melt and fluid phases simultaneously. This approach emphasises the arguably most fundamental behavior of porphyry-mineralising arc magmas: the positive feedback between crystallization and massive production of H_2O-dominant fluid over a narrow P-T interval ('second boiling'; Burnham and Ohmoto, 1980). The high concentration of H_2O in arc magmas justifies ignoring minor CO_2 which is generally insufficient to drive sulfide decomposition at mid- to lower-crustal pressures (Fig. S1). Our computational approach can be readily extended to future models which should incorporate the distribution and speciation of S as well as chalcophile trace-elements between coexisting S-bearing silicate melt, solid and liquid sulfide, other minerals, and hydrothermal fluids including Cl as the next-most influential fluid component (Dolejs and Zajacz, 2018).

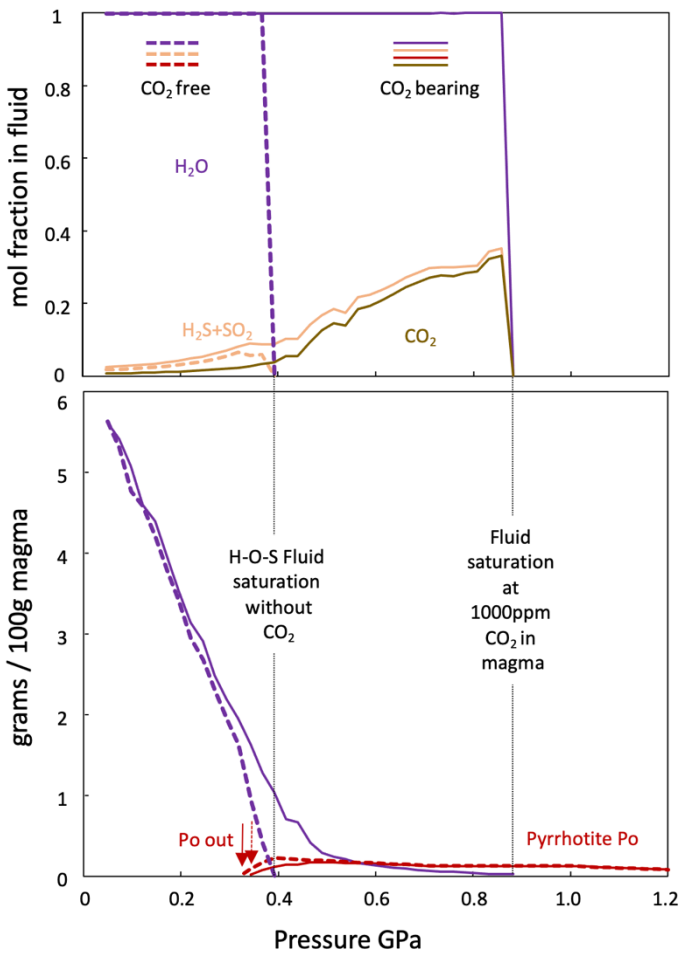

Figure S1: The calculated effect of CO_2 for the near-adiabatic *P-T* transect shown in Figures 2B and D of the main paper, including the addition of 1000ppm CO_2. CO_2 solubility in the melt was modelled by assuming Henryian behavior and matching the solubilities reported by Morizet et al. (2010), which extends older experimental data that are commonly used in fluid - melt modelling studies (e.g., Mungall et al., 2015; Yao and Mungall, 2020). Fluid composition (top) and phase quantities (bottom) for the CO_2 bearing system are shown by solid lines, compared with those of the simplified H-O-S system shown with dashed lines. CO_2 addition causes fluid saturation at higher pressure, but the fluid quantity is too small to significantly affect the abundance of magmatic sulfides, which become destabilized by massive H_2O exsolution closer to the solidus. Most importantly, the pressure at which de-sulfidation of entrained sulfide is completed is practically unchanged (small arrows indicating "Po out"). Thus magmatic CO_2 has a minor, albeit moderating, influence on the sulfide stability predicted for the CO_2-free system. We ignored this second-order complexity and consider only the H-O-S limiting model because, unlike iron sulfide, the C-content of the melt adds an arbitrary degree of freedom that is not directly constrained by the presence of an additional phase.

For the supercritical H-O-S or C-H-O-S fluid, the Hybrid Molecular Fluid model following Connolly (1995) was used: https://perplex.ethz.ch/Perple_X_generic_hyrbid_fluid_EoS.html

Crystalline solid-solution models are from (or as recommended by) Holland et al. (2018) based on endmember thermodynamic data for minerals from the ds6.33 revision of Holland and Powell (2011). MSS or pyrrhotite (Po(HP)) is modelled as solid solution with the endmembers trot = FeS and trov = $Fe_{0.88}S$. In the binary Fe-S system solid MSS is stable to ~ 1200°C (e.g., Kitakaze et al., 2016) and a Cu-Ni-bearing sulfide melt is stabilised to lower temperatures, but these minor components contribute less than 10% to natural (possibly composite liquid + solid) magmatic sulfide particles (e.g., Rottier et al., 2020). We suppressed amphibole (cAmph(G)) and ilmenite solution (Ilm(WPH)) because these models have unrealistically high stable ferric iron-contents and destabilize magnetite even at the most oxidising conditions, counter to geological observation. The 'Mafics' (= pyroxenes ± olivine ± biotite shown in Figure 2) will in reality be dominated by amphibole in water-rich oxidised arc magmas considered here (Nandedkar et al., 2014; Loucks, 2021).

For the magma composition we chose the average continental arc basalt of Rezeau and Jagoutz (2020) and Schmidt and Jagoutz (2017). Their anhydrous model composition (Table S1) was varied by adding a fixed quantity of FeS (0.5 wt%) and variable concentrations of H_2O between 3 and 6 wt% (a range considered to be ideal for subsequent hydrothermal ore formation; Chiaradia, 2020), and by varying the bulk Fe^{III}/Fe^{tot} ratio between 0.18 and 0.48 at given FeO^{tot}. This variation covers the range of Fe^{III}/Fe^{tot} reported from modelling-independent Fe-XANES measurements on silicate melt inclusions (~ 0.15 – 0.4; (Kelley and Cottrell, 2009; Brounce et al., 2022).

Fe^{III}/Fe^{tot} in the bulk system dominates the redox potential of the magma, which can be measured by oxygen fugacity relative to the quartz – fayalite – magnetite equilibrium ($\Delta logfO_2$(QFM); (Mavrogenes and O'Neill, 1999). Gibbs energy minimization emphasizes that the trace volatile components (O_2, H_2) are dominated by equilibria between major ferrous and ferric components of oxides, silicates and the melt and modified by reactions among minor sulfur species: SO_2 and H_2S in the fluid and magmatic FeS and sulfate (here modelled by anhydrite, in reality partly dissolved in melt). We deliberately avoid fixing $\Delta logfO_2$(QFM) (as commonly done using the MELTS model following Ghiorso and Sack, 1995; e.g., Rezeau and Jagoutz, 2020), to illustrate the natural competition among the main redox-sensitive phases. The model of Holland et al. (2018) for Fe components in the silicate melt satisfies experimental relations between fO_2 and Fe^{III}/Fe^{tot} (Kress and Carmichael, 1991; O'Neill et al., 2006) and resulting $\Delta logfO_2$(QFM) between +1.0 and +2.2 for the chosen range of bulk compositions are consistent with oxybarometer results of natural porphyry-copper mineralizing magmas as reviewed by Richards (2015) and Loucks et al. (2020). Figure S2 shows Fe^{III}/Fe^{tot} variations along the P-T transect of Figure 2D of the paper and the resulting $\Delta logfO_2$(QFM).

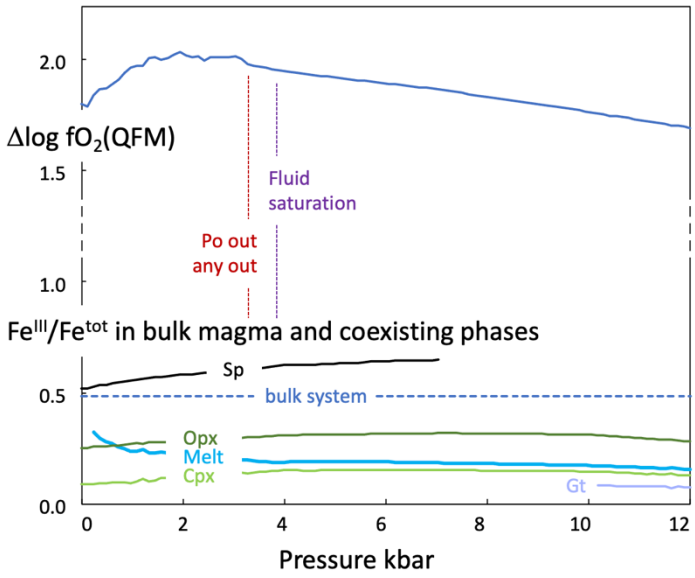

Figure S2: Variation of $\Delta logfO_2$(QFM) (upper part of diagram) and the Fe^{III}/Fe^{tot} ratio in silicate and oxide phases at given bulk ratio for the system (lower part), for the same model magma and P-T transect as shown in Figure 2 of the paper. The ratio in the silicate melt is lower than in the bulk system, not only because of the stabilization of Fe^{III}-rich spinel at pressures below ~7 kbar but also because of the competition of O between the major phases and minor pyrrhotite and anhydrite at all pressures above 'Po out' and 'any out'.

The thermodynamic database files (hp633ver.dat), solid solution properties (solution_model.dat) and computational options such as grid resolution (perplex_options.dat) are stored in a folder Perple_X_6_Cu at https://polybox.ethz.ch/index.php/s/qwnROpGuNQBWgjf, which also contains all job definition files (e.g., RJox3=2x2_6H2O_Po.dat — see box below for the job example used to calculate Figures 2, S1, S2) as well as the resulting output and plot files. Parts of this repository will be published at https://www.research-collection.ethz.ch.

The two gray P-T transects in Figure 2B along which phase proportions depicted in 2A and 2C are based on Annen et al. (2006) who coined the now widely used term 'hot zone' as a region of lower-crustal magma storage and differentiation.

Job file example RJox3=2x2_6H2O_Po.dat

```
hp633ver.dat     thermodynamic data file.        |THIS INCLUDES THE MELT SPECIES OF  HOLLAND ET AL JPET 2018
print                        | no_print suppresses print output
plot                         | obsolete 6.8.4+
solution_model.dat     | solution model file, blank = none
RezeauJagoutz'2020_Calcalkaline_Basalt_Fe(III)=2xFe(II) 6%H2O  Po(HP)=trov-trot-ss
perplex_option.dat     | Perple_X option file
   5 calculation type: 0- composition, 1- Schreinemakers, 3- Mixed, 4- swash, 5- gridded min, 7- 1d fract, 8- gwash, 9- 2d fract,
10- 7 w/file input, 11- 9 w/file input, 12- 0d infiltration
   0 unused place holder, post 06
   0 unused place holder, post 06
   0 unused place holder, post 06
   0 unused place holder, post 06
   0 unused place holder, post 06
   0 unused place holder, post 06
   0 unused place holder, post 06
   0 unused place holder, post 06
   0 unused place holder, post 06
   0 number component transformations
  20 number of components in the data base
   0 component amounts, 0 - mole, 1 mass
   0 unused place holder, post 06
   0 unused place holder, post 06
   0 unused place holder, post 05
   0 ifug EoS for saturated phase
   2 gridded minimization dimension (1 or 2)
   0 special dependencies: 0 - P and T independent, 1 - P(T), 2 - T(P)
 0.00000     0.00000     0.00000     0.00000     0.00000     Geothermal gradient polynomial coeffs.

begin thermodynamic component list
SiO2    1   .7880       0.00000     0.00000     molar  amount
TiO2    1   .0116       0.00000     0.00000     molar  amount
Al2O3 1   .1440       0.00000     0.00000     molar  amount
O2      1   .0108       0.00000     0.00000     molar  amount
FeO     1   .1172       0.00000     0.00000     molar  amount
MgO     1   .2385       0.00000     0.00000     molar  amount
CaO     1   .1651       0.00000     0.00000     molar  amount
Na2O    1   .0423       0.00000     0.00000     molar  amount
K2O     1   .0104       0.00000     0.00000     molar  amount
H2O     1   .3127       0.00000     0.00000     molar  amount
S2      1   .0027       0.00000     0.00000     molar  amount
end thermodynamic component list

begin saturated component list
end saturated component list

begin saturated phase component list
end saturated phase component list

begin independent potential/fugacity/activity list
end independent potential list
```

```
[continued]

begin solution phase list
Chl(W)
melt(HGP)
HOS-Fluid
| cAmph(G)  Suppressing this amphibole containing overly stable riebeckite component
Cpx(HGP)
Opx(HGP)
Sp(HGP)
|  Ilm(WPH)  Suppressing this ilmenite containing overly stable hematite component
Bi(HGP)
feldspar
Gt(HGP)
Mica(W)
Crd(HGP)
O(HGP)
Ep(HP11)
Po(HP)     |solid solution of trot=FeS and trov=Fe0.88S endmembers
end solution phase list

  12000.0      1473.00      0.00000      0.00000      0.00000    max p, t, xco2, mu_1, mu_2
    1.00       973.000      0.00000      0.00000      0.00000    min p, t, xco2, mu_1, mu_2
 0.00000       0.00000      0.00000      0.00000      0.00000    unused place holder post 06

 2  1  4  5  3   indices of 1st & 2nd independent & sectioning variables
```

H-S-metal diffusion in silicate melt and selective metal precipitation

We cite Zhang and Ni (2010) for the fast diffusion of H compared to most metal components. This recent review also discusses the difficulty of quantifying the diffusion of H_2O and H_2 as molecular entities controlling magma devolatilization and redox equilibria. Comparison with S diffusion is further explored by Lierenfeld et al. (2018) who show that H_2S diffusion is comparably fast whereas SO_2 and SO_4 diffuse much more slowly than H_2O in silicate melt. Also Cu^+ diffuses comparably fast, similar to H species (Ni et al., 2017), so for Cu alone the mechanism of direct transfer from sulfide phase to fluid (Fig. 4) may not be decisive, but it is probably essential for wholesale transfer of Cu together with larger ions including Au, Pd and Pt. This process was proposed to explain the similarity of Au/Cu ratios between sulfides, fluids and bulk ore in some porphyry systems (Halter et al., 2002; Halter et al., 2005). Other deposits where metals ratios differ between magmatic sulfides and final ore show that subsequent selective metal precipitation is equally important (e.g., porphyry Au deposits; Murakami et al., 2010; Rottier et al., 2019). Because of the importance of selective precipitation, the low concentration of Au in some, and of Pt and Pd in most porphyry deposits (Cocker et al., 2015; Park et al., 2021) is not a conclusive argument against their transfer from magmatic sulfides to hydrothermal fluid, given their high solubility in magmatic-hydrothermal fluids (Simon and Pettke, 2009; Sullivan et al., 2022).

Cu,Ag mass-balance estimation

Published fractionation models have calculated the mass balance of S and chalcophile trace elements such as Cu and Ag between evolving silicate melt, iron sulfide (MSS), sulfide melt and fluid (e.g., Rottier et al., 2019; Yao and Mungall, 2020). Here we explore physical co-transportation of sulfide with the silicate melt, so we estimate the fraction of Cu and Ag

residing in sulfide for a fixed total amount of the trace element (e.g., Cu(total)) and a fixed ratio of sulfide: silicate melt (R-factor) corresponding to 0.2 to 0.5 wt% FeS. Then Cu(sulfide) = Cu(total)*D*(R+1)/(R+D), where D is the distribution coefficient, e.g., Cu(sulfide)/Cu(silicate melt) (Campbell and Naldrett, 1979; Richards, 2015). We assume D = 400 for Cu and 60 for Ag, assuming the sulfide is MSS, but values would be higher if some of the sulfide was present as sulfide melt (Li and Audétat, 2012) which would make the process of sulfide entrainment even more effective for chalcophile metal transport. This is a simplified first-order estimation compared to earlier mass-balance modelling that explicitly consider sulfide phase state, sulfide phase composition, and the partitioning of Cu compared to the more chalcophile precious metals (Cocker et al., 2015; Mungall et al., 2015; Yao and Mungall, 2020). However, our estimate presents a limiting case showing that sulfide entrainment can avoid depletion of ore forming components from evolving arc magmas.

Comments on Cu in magmatic fluids and possible dispersal to the hydrosphere

A review of Cu concentrations in natural magmatic fluids exceeds the size limitation of this paper, so a few supplementary references are cited here in support of the speculation that magmatic fluids may contribute significantly to dispersion of Cu from continental magmatic arcs to the hydrosphere. The solubility of Cu, but also of the even more strongly chalcophile trace-elements Au, Pt and Pd is so high at magmatic temperatures (Simon and Pettke, 2009; Sullivan et al., 2022) that all are likely to be highly undersaturated in primary magmatic fluids, which favors their wholesale transfer from decomposing sulfide to fluid (Halter et al., 2005). In natural fluid inclusions, high Cu concentrations are widespread in intermediate-density ('supercritical') fluids of ore-forming as well as barren upper-crustal plutons (Audétat, 2019) including subvolcanic ejecta in arc volcanoes (e.g., Fiedrich et al., 2020). Cu contents approaching percent levels are observed in vapor inclusions of volcanic phenocrysts (Lowenstern et al., 1991; Zajacz and Halter, 2009). Hot volcanic fumaroles are commonly metal-rich and were previously proposed to make a significant contribution to global S and Cu flux to atmosphere and hydrosphere (Nadeau et al., 2010; Wallace and Edmonds, 2011; Edmonds et al., 2018). Submarine volcanics and oceanic arcs under significant seawater pressure have a better chance to preserve magmatic sulfide particles even in the glassy matrix of quenched volcanics, compared to subaerial volcanics (Jenner et al., 2010). For example, Li et al. (2019) reported relict magmatic sulfides in dredged dacites and more primitive enclaves and cumulates of the Okinawa back-arc trough and linked their partial composition to the formation of hydrothermal sulfides in black smoker deposits.

Our thermodynamic calculations imply that the expulsion of S and chalcophile metals by hydrous sulfide-saturated magmas is most efficient from intrusions crystallizing at some depth in the upper crust (~ 3 - 10 km), in regions of thick continental crust that are most likely to promote earlier fractionation to high water content (Loucks, 2021). It should be noted that only a small fraction of their hydrothermal Cu is focussed into rare porphyry copper deposits, which themselves are geologically short-lived copper accumulations that are typically recycled by weathering and erosion within ~ 100 Ma (Wilkinson and Kesler, 2009). By far the greatest part of hydrothermal metals will never be concentrated but dispersed into deep groundwater and basement brines, allowing the possibility that a

significant fraction of chalcophile trace metals might become recycled via hydrosphere and oceanic sediments that are eventually subducted.

Supplementary References

Annen, C., Blundy, J. D., and Sparks, R. S. J., 2006, The genesis of intermediate and silicic magmas in deep crustal hot zones: Journal of Petrology, v. 47, p. 505-539, doi:10.1093/petrology/egi084.

Audétat, A., 2019, The metal content of magmatic-hydrothermal fluids and Its relationship to mineralization potential: Economic Geology, v. 114, p. 1033-1056, doi:10.5382/econgeo.4673.

Brounce, M., Stolper, E., and Eiler, J., 2022, The mantle source of basalts from Reunion Island is not more oxidized than the MORB source mantle: Contributions to Mineralogy and Petrology, v. 177, doi:10.1007/s00410-021-01870-w.

Burnham, C. W., and Ohmoto, H., 1980, Late-stage processes of felsic magmatism: Mining Geology Special Issue, p. 1-11

Campbell, I. H., and Naldrett, A. J., 1979, Influence of silicate - sulfide ratios on the geochemistry of magmatic sulfides: Economic Geology, v. 74, p. 1503-1506, doi:DOI 10.2113/gsecongeo.74.6.1503.

Chiaradia, M., 2020, How Much Water in Basaltic Melts Parental to Porphyry Copper Deposits?: Frontiers in Earth Science, v. 8, doi:10.3389/feart.2020.00138.

Cocker, H. A., Valente, D. L., Park, J. W., and Campbell, I. H., 2015, Using platinum group elements to identify sulfide saturation in a porphyry Cu system: the El Abra porphyry Cu deposit, Northern Chile: Journal of Petrology, v. 56, p. 2491-2514, doi:10.1093/petrology/egv076.

Connolly, J. A. D., 1995, Phase-diagram methods for graphitic rocks and application to the system C-O-H-FeO-TiO2-SiO2: Contributions to Mineralogy and Petrology, v. 119, p. 94-116

-, 2005, Computation of phase equilibria by linear programming: A tool for geodynamic modeling and its application to subduction zone decarbonation: Earth and Planetary Science Letters, v. 236, p. 524-541, doi:10.1016/j.epsl.2005.04.033.

Cox, D., Watt, S. F. L., Jenner, F. E., Hastie, A. R., Hammond, S. J., and Kunz, B. E., 2020, Elevated magma fluxes deliver high-Cu magmas to the upper crust: Geology, v. 48, p. 957-960, doi:10.1130/g47562.1.

De Bremond d'Ars, J., Arndt, N. T., and Hallot, E., 2001, Analog experimental insights into the formation of magmatic sulfide deposits: Earth and Planetary Science Letters, v. 186, p. 371-381

Dolejs, D., and Zajacz, Z., 2018, Halogens in silicic magmas and their hydrothermal systems: Role of Halogens in Terrestrial and Extraterrestrial Geochemical Processes: Surface, Crust, and Mantle, p. 431-543, doi:10.1007/978-3-319-61667-4_7.

Edmonds, M., Mather, T. A., and Liu, E. J., 2018, A distinct metal fingerprint in arc volcanic emissions: Nature Geoscience, v. 11, p. 790-+, doi:10.1038/s41561-018-0214-5.

Fiedrich, A. M., Heinrich, C. A., and Bachmann, O., 2020, Evolution from magmatic to hydrothermal activity beneath the Cerro Escorial volcano (NW Argentina) as sampled by erupted quartz and brines: Lithos, v. 374, p. 105706 doi:10.1016/j.lithos.2020.105706.

Fortin, M. A., Riddle, J., Desjardins-Langlais, Y., and Baker, D. R., 2015, The effect of water on the sulfur concentration at sulfide saturation (SCSS) in natural melts: Geochimica et Cosmochimica Acta, v. 160, p. 100-116, doi:10.1016/j.gca.2015.03.022.

Ghiorso, M. S., and Sack, R. O., 1995, Chemical mass transfer in magmatic processes 4. A revised and intenally consistent thermodynamic model for the interpolation ad extrapolation of liquid - solid equilibria in magmatic systems at elevated temperatures and pressures: Contributions to Mineralogy and Petrology, v. 119, p. 197-212, doi:10.1007/bf00307281.

Giordano, D., Russell, J. K., and Dingwell, D. B., 2008, Viscosity of magmatic liquids: A model: Earth and Planetary Science Letters, v. 271, p. 123-134, doi:10.1016/j.epsl.2008.03.038.

Halter, W., Heinrich, C., and Pettke, T., 2005, Magma evolution and the formation of porphyry Cu-Au ore fluids: evidence from silicate and sulfide melt inclusions: Mineralium Deposita, v. 39, p. 845-863, doi:10.1007/s00126-004-0457-5.

Halter, W. E., Pettke, T., and Heinrich, C. A., 2002, The origin of Cu/Au ratios in porphyry-type ore deposits: Science, v. 296, p. 1844-1846

Holland, T. J. B., and Powell, R., 2011, An improved and extended internally consistent thermodynamic dataset for phases of petrological interest, involving a new equation of state for solids: Journal of Metamorphic Geology, v. 29, p. 333-383, doi:10.1111/j.1525-1314.2010.00923.x.

Iacovino, K., and Till, C. B., 2018, DensityX: A program for calculating the densities of magmatic liquids up to 1627°C and 30 kbar: Volcanica: Presses universitaires de Strasbourg, v. 2, p. 1-10, doi:doi: 10.30909/vol.02.01.0110.

Jenner, F. E., O'Neill, H. S. C., Arculus, R. J., and Mavrogenes, J. A., 2010, The magnetite crisis in the evolution of arc-related magmas and the initial concentration of Au, Ag and Cu: Journal of Petrology, v. 51, p. 2445-2464, doi:10.1093/petrology/egq063.

Jugo, P. J., 2009, Sulfur content at sulfide saturation in oxidized magmas: Geology, v. 37, p. 415-418, doi:10.1130/g25527a.1.

Kelley, K. A., and Cottrell, E., 2009, Water and the oxidation state of subduction zone magmas: Science, v. 325, p. 605-607, doi:10.1126/science.1174156.

Kitakaze, A., Machida, T., and Komatsu, R., 2016, Phase relations in the Fe-Ni-S system from 875 to 650°C: Canadian Mineralogist, v. 54, p. 1175-1186, doi:10.3749/canmin.1500087.

Kress, V., Greene, L. E., Ortiz, M. D., and Mioduszewski, L., 2008, Thermochemistry of sulfide liquids IV: density measurements and the thermodynamics of O-S-Fe-Ni-Cu liquids at low to moderate pressures: Contributions to Mineralogy and Petrology, v. 156, p. 785-797, doi:10.1007/s00410-008-0315-z.

Kress, V. C., and Carmichael, I. S. E., 1991, The compressibility of silicate liquids containing Fe2O3 and the effect of composition, temperature, oxygen fugacity and pressure on their redox states Contributions to Mineralogy and Petrology, v. 108, p. 82-92, doi:10.1007/bf00307328.

Li, Z. G., Chu, F. Y., Zhu, J. H., Ding, Y., Zhu, Z. M., Liu, J. Q., Wang, H., Li, X. H., Dong, Y. H., and Zhao, D. N., 2019, Magmatic sulfide formation and oxidative dissolution in the SW Okinawa Trough: A precursor to metal-bearing magmatic fluid: Geochimica et Cosmochimica Acta, v. 258, p. 138-155, doi:10.1016/j.gca.2019.05.024.

Lierenfeld, M. B., Zajacz, Z., Bachmann, O., and Ulmer, P., 2018, Sulfur diffusion in dacitic melt at various oxidation states: Implications for volcanic degassing: Geochimica Et Cosmochimica Acta, v. 226, p. 50-68, doi:10.1016/j.gca.2018.01.026.

Liu, Y. N., Samaha, N. T., and Baker, D. R., 2007, Sulfur concentration at sulfide saturation (SCSS) in magmatic silicate melts: Geochimica et Cosmochimica Acta, v. 71, p. 1783-1799, doi:10.1016/j.gca.2007.01.004.

Loucks, R. R., Fiorentini, M. L., and Henriquez, G. J., 2020, New Magmatic Oxybarometer Using Trace Elements in Zircon: Journal of Petrology, v. 61, doi:ARTN egaa034 10.1093/petrology/egaa034.

Lowenstern, J. B., Mahood, G. A., Rivers, M. L., and Sutton, S. R., 1991, Evidence for Extreme Partitioning of Copper into a Magmatic Vapor-Phase: Science, v. 252, p. 1405-1409, doi:DOI 10.1126/science.252.5011.1405.

Mavrogenes, J. A., and O'Neill, H. S. C., 1999, The relative effects of pressure, temperature and oxygen fugacity on the solubility of sulfide in mafic magmas: Geochimica Et Cosmochimica Acta, v. 63, p. 1173-1180, doi:10.1016/s0016-7037(98)00289-0.

Morizet, Y., Paris, M., Gaillard, F., and Scaillet, B., 2010, C-O-H fluid solubility in haplobasalt under reducing conditions: An experimental study: Chemical Geology, v. 279, p. 1-16, doi:10.1016/j.chemgeo.2010.09.011.

Murakami, H., Seo, J. H., and Heinrich, C. A., 2010, The relation between Cu/Au ratio and formation depth of porphyry-style Cu-Au +/- Mo deposits: Mineralium Deposita, v. 45, p. 11-21, doi:10.1007/s00126-009-0255-1.

Nandedkar, R. H., Ulmer, P., and Müntener, O., 2014, Fractional crystallisation of primitive, hydrous arc magmas: an experimental study at 0.7 GPa: Contrib. Mineral. Petrol., v. 167, p. 1015, doi:10.1007/s00410-014-1015-5.

Ni, P., Zhang, Y. X., Simon, A., and Gagnon, J., 2017, Cu and Fe diffusion in rhyolitic melts during chalcocite "dissolution": Implications for porphyry ore deposits and tektites: American Mineralogist, v. 102, p. 1287-1301, doi:10.2138/am-2017-5885.

Nishida, K., Ohtani, E., Urakawa, S., Suzuki, A., Sakamaki, T., Terasaki, H., and Katayama, Y., 2011, Density measurement of liquid FeS at high pressures using synchrotron X-ray absorption: American Mineralogist, v. 96, p. 864-868, doi:10.2138/am.2011.3616.

O'Neill, H. S. C., Berry, A. J., McCammon, C. C., Jayasuriya, K. D., Campbell, S. J., and Foran, G., 2006, An experimental determination of the effect of pressure on the Fe3+/Sigma Fe ratio of an anhydrous silicate melt to 3.0 GPa: American Mineralogist, v. 91, p. 404-412, doi:10.2138/am.2005.1929.

Rottier, B., Audetat, A., Kodera, P., and Lexa, J., 2020, Magmatic evolution of the mineralized Stiavnica volcano (Central Slovakia): Evidence from thermobarometry, melt inclusions, and sulfide inclusions: Journal of Volcanology and Geothermal Research, v. 401, p. ARTN 106967, doi:10.1016/j.jvolgeores.2020.106967.

Schmidt, M. W., and Jagoutz, O., 2017, The global systematics of primitive arc melts: Geochemistry Geophysics Geosystems, v. 18, p. 2817-2854, doi:10.1002/2016gc006699.

Simon, A. C., and Pettke, T., 2009, Platinum solubility and partitioning in a felsic melt-vapor-brine assemblage: Geochimica Et Cosmochimica Acta, v. 73, p. 438-454, doi:10.1016/j.gca.2008.10.020.

Turner, S., and Costa, F., 2007, Measuring timescales of magmatic evolution: Elements, v. 3, p. 267-272, doi:10.2113/gselements.3.4.267.

Wallace, P. J., and Edmonds, M., 2011, The sulfur budget in magmas: Evidence from melt inclusions, submarine glasses, and volcanic gas emissions: Rev Mineral Geochem: Sulfur in Magmas and Melts: Its Importance for Natural and Technical Processes, v. 73, p. 215-246, doi:10.2138/rmg.2011.73.8.

Wilkinson, B. H., and Kesler, S. E., 2009, Quantitative identification of metallogenic epochs and provinces: application to Phanerozoic porphyry copper deposits: Economic Geology, v. 104, p. 607-622

Yao, Z. S., Mungall, J. E., and Qin, K. Z., 2019, A preliminary model for the migration of sulfide droplets in a magmatic conduit and the significance of volatiles: Journal of Petrology, v. 60, p. 2281-2315, doi:10.1093/petrology/egaa005.

Zajacz, Z., and Halter, W., 2009, Copper transport by high temperature, sulfur-rich magmatic vapor: Evidence from silicate melt and vapor inclusions in a basaltic andesite from the Villarrica volcano (Chile): Earth and Planetary Science Letters, v. 282, p. 115-121, doi:10.1016/j.epsl.2009.03.006.